AGU PUBLICATIONS

JGR

Journal of Geophysical Research: Oceans

RESEARCH ARTICLE

10.1002/2015JC010700

Key Points:
- Arctic export efficiency displays large variability
- Blooming diatoms and *Phaeocystis* sp. have the highest export efficiency
- More work is needed on upper mesopelagic remineralization in the Arctic

Supporting Information:
- Supporting Information S1

Correspondence to:
F. A. C. Le Moigne,
flemoigne@geomar.de

Citation:
Moigne, F. A. C., et al. (2015), Carbon export efficiency and phytoplankton community composition in the Atlantic sector of the Arctic Ocean, *J. Geophys. Res. Oceans*, *120*, 3896–3912, doi:10.1002/2015JC010700.

Received 6 JAN 2015
Accepted 27 APR 2015
Accepted article online 4 MAY 2015
Published online 1 JUN 2015

Carbon export efficiency and phytoplankton community composition in the Atlantic sector of the Arctic Ocean

Frédéric A. C. Le Moigne[1,2], Alex J. Poulton[1], Stephanie A. Henson[1], Chris J. Daniels[3], Glaucia M. Fragoso[3], Elaine Mitchell[4], Sophie Richier[3], Benjamin C. Russell[3], Helen E. K. Smith[3], Geraint A. Tarling[5], Jeremy R. Young[6], and Mike Zubkov[1]

[1]National Oceanography Centre, European Way, Southampton, UK, [2]GEOMAR, Helmholtz Centre for Ocean Research, Kiel, Germany, [3]University of Southampton, European Way, Southampton, UK, [4]Scottish Association for Marine Sciences, Oban, Argyll, UK, [5]British Antarctic Survey, Natural Environment Research Council, High Cross, Cambridge, UK, [6]University College London, London, UK

Abstract Arctic primary production is sensitive to reductions in sea ice cover, and will likely increase into the future. Whether this increased primary production (PP) will translate into increased export of particulate organic carbon (POC) is currently unclear. Here we report on the POC export efficiency during summer 2012 in the Atlantic sector of the Arctic Ocean. We coupled 234-thorium based estimates of the export flux of POC to onboard incubation-based estimates of PP. Export efficiency (defined as the fraction of PP that is exported below 100 m depth: *ThE*-ratio) showed large variability (0.09 ± 0.19–1.3 ± 0.3). The highest *ThE*-ratio (1.3 ± 0.3) was recorded in a mono-specific bloom of *Phaeocystis pouchetii* located in the ice edge. Blooming diatom dominated areas also had high *ThE*-ratios (0.1 ± 0.1–0.5 ± 0.2), while mixed and/or pre-bloom communities showed lower *ThE*-ratios (0.10 ± 0.03–0.19 ± 0.05). Furthermore, using oxygen saturation, bacterial abundance, bacterial production, and zooplankton oxygen demand, we also investigated spatial variability in the degree to which this sinking material may be remineralized in the upper mesopelagic (<300 m). Our results suggest that blooming diatoms and *P. pouchetii* can export a significant fraction of their biomass below the surface layer (100 m) in the open Arctic Ocean. Also, we show evidence that the material sinking from a *P. pouchetii* bloom may be remineralized (>100 m) at a similar rate as the material sinking from diatom blooms in the upper mesopelagic, contrary to previous findings.

1. Introduction

Climate change is impacting the Arctic Ocean, with the most obvious manifestation of these changes being the reduction in summer sea-ice cover [*Boé et al*., 2009]. Modeling and observational studies imply that reduced sea-ice in the future will strengthen Arctic primary production (PP) [*Arrigo et al*., 2008; *Pabi et al*., 2008]. The biological carbon pump (BCP) is an important component of the global carbon (C) cycle, mainly driven by the sinking of organic material from the sunlit upper layer of the ocean [*Boyd and Trull*, 2007]. The fraction of PP that is exported below the euphotic zone (Ez) or below the surface layer (export/primary production, or export efficiency, *ThE*(*Ez*)-ratio [*Buesseler*, 1998; *Buesseler and Boyd*, 2009]) is a key determinant in how efficiently the BCP sequesters C to depth [*Buesseler and Boyd*, 2009]. Furthermore, the fraction of this material, which successfully transits deeper into the water column (upper mesopelagic zone) where the majority of remineralization of sinking particulate organic material occurs [*Buesseler and Boyd*, 2009; *Giering et al*., 2014], is indicative of BCP efficiency [*Buesseler and Boyd*, 2009]. The specific ecosystem related processes that drive the considerable variability observed in *ThE*(Ez)-ratios and further down into the upper mesopelagic remain largely unknown [*Buesseler and Boyd*, 2009; *Giering et al*., 2014; *Henson et al*., 2011] for much of the polar oceans.

Although a large body of literature reporting estimates of POC export fluxes using various techniques is available in the Arctic Ocean [*Cai et al*., 2010; *Chen et al*., 2003; *Coppola et al*., 2002; *Lalande et al*., 2011, 2007, 2008; *Moran et al*., 1997; *Moran and Smith*, 2000; *Reigstad and Wassmann*, 2007; *Wassmann et al*., 1990], little is known about the variability of the *ThE*(Ez)-ratio [*Buesseler*, 1998; *Buesseler and Boyd*, 2009]. *Cai et al*. [2010] and *Chen et al*. [2003] both report ratios of POC export flux to PP in the central Arctic Ocean, but this ratio has yet to be estimated in the deep ocean rather than over shelf waters, or over gradients of

ice to ice-free conditions. Export efficiency from such regions and associated blooms has been estimated before, but with limited information on the plankton community composition [*Cai et al*., 2010; *Chen et al*., 2003] and/or with an export efficiency calculation methodology different from the *ThE*(Ez)-ratio approach [*Reigstad et al*., 2008; *Smith et al*., 1991], hence preventing direct comparisons. In cold waters, the coupling between surface carbon export and PP is known to be highly variable [*Henson et al*., 2011] and the specific processes that drive variability in *ThE*(Ez)-ratio in the Arctic Ocean remain elusive [*Buesseler and Boyd*, 2009]. One possible explanation for the variability in *ThE*(Ez)-ratio in cold high latitudes is the strong seasonality in phytoplankton bloom evolution and seasonal succession in phytoplankton functional types observed at high latitudes [*Boyd and Newton*, 1995, 1999].

Blooms of various phytoplankton groups have been reported in the Atlantic sector of the Arctic Ocean and Fram Strait, including diatoms [*Gradinger and Baumann*, 1991], coccolithophores [*Smyth et al*., 2004], and the colonial haptophyte *Phaeocystis* spp. [*Smith et al*., 1991; *Wassmann*, 1994]. However, it is unknown whether these phytoplankton groups result in similar *ThE*(Ez)-ratios when they are present and/or dominating the community composition. There are, therefore, grounds to hypothesize that some of the variability observed in *ThE*(Ez)-ratios may be explained by phytoplankton composition. Furthermore, it is not clear whether sinking material derived from different phytoplankton groups experience a similar amount of heterotrophic respiration once it has entered the upper mesopelagic zone [*Buesseler and Boyd*, 2009]. This aspect is critical if one wants to predict the future changes in the open Arctic BCP and, further, the influence of the Arctic Ocean on climate regulation.

To date, we know that future changes in temperature, CO_2, light regime, and macro(micro)-nutrient inputs may all induce important changes in both primary production and phytoplankton community composition in the Arctic [*Bopp et al*., 2005; *Coello-Camba et al*., 2014; *Perrette et al*., 2011; *Popova et al*., 2010, 2012; *Vancoppenolle et al*., 2013]. Unless clear links are established between phytoplankton community composition and carbon export metrics, such as the *ThE*(Ez)-ratio [*Buesseler and Boyd*, 2009], it will be difficult to predict how these changes will impact the efficiency of the Arctic BCP.

Here we surveyed variability in the *ThE*-ratio (as we defined and define the depth of integration for this study to be 100 m) [*Buesseler*, 1998] in the Atlantic sector of the Arctic Ocean and the Fram Strait where POC export flux estimates are rare [*Le Moigne et al*., 2013a], using the ^{234}Th technique (to estimate export of POC) and onboard ^{14}C incubations (to determine PP). These parameters were related to the major phytoplankton groups present in the water column during the survey period. Furthermore, oxygen saturation, bacterial production, and zooplankton oxygen demand are used to qualitatively assess to what extent this sinking material may be remineralized in the upper mesopelagic (<300 m). This represents the first attempt to estimate *ThE*-ratio and upper mesopelagic remineralization in the Atlantic sector of the Arctic Ocean.

2. Methods

2.1. Sampling and Analysis of Ancillary Data

The cruise took place onboard the *R.R.S*. James Clark Ross (British Antarctic Survey) in June 2012 as part of the UK's Ocean Acidification programme. Sampling took place from 12th June to the 1st July 2012 in the Greenland, Norwegian and Barents Seas (Figure 1; station positions are given in Table 1). Water samples were collected with Niskin bottles via deployment of a SeaBird CTD system. Dissolved oxygen (DO) profiles were taken from the CTD optode and calibrated against discrete O_2 measurements performed using a semi-automated whole bottle Winkler titration unit with spectrophotometric end point detection manufactured by SIS (http://www.sis-germany.com) following *Dickson* [1994] at all discrete depths. Samples (0.1–0.5 L) for chlorophyll-*a* (Chl-*a*) analysis were collected in the middle of the mixed layer (10–25 m, see Table 1) and filtered onto GF/F filters and then extracted into 90% acetone for 24 h in the dark before analysis with a fluorometer (Trilogy; Turner Designs). Samples for analysis of particulate organic carbon (POC) (0.5–1 L) were collected and analyzed following protocols described in *Le Moigne et al*. [2013b]. Raw fluorescence from the CTD fluorometer was cross-calibrated with discrete measurements of Chl-*a*.

2.2. Phytoplankton Community Composition, Abundance, and Biomass

Water samples (100–250 mL) were collected from the middle of the mixed layer (10–25 m, see Table 1) from each station and preserved with 2% final concentration acidic Lugol's solution for later analysis of

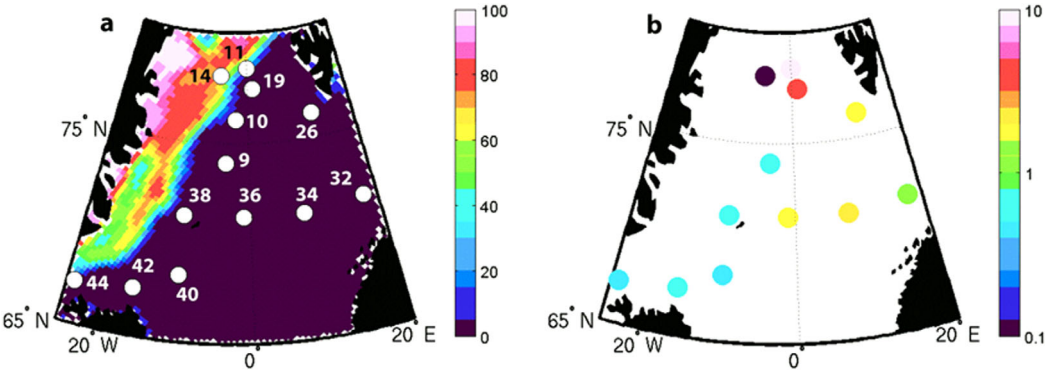

Figure 1. (a) Percentage (%) sea ice concentration in June 2012 after *Cavalieri et al*., [1996, updated yearly]. Sea ice concentration data are taken from the Nimbus-7 SMMR and DMSP SSM/I-SSMIS passive microwave sensors and downloaded from www.nsidc.org. Station numbers are indicated. (b) Surface (see Table 1 for depth) Chlorophyll-*a* concentration (mg m^{-3}).

microplankton community structure. Subsamples (10–50 mL) were settled overnight in 10–50 mL HydroBios settling chambers following [*Uttermohl*, 1958] and microplankton were enumerated using a SP-95-I inverted light microscope (Brunel Ltd). Biomass of each phytoplankton species was calculated following *Poulton et al*. [2010, 2007] and is presented in Table 1.

2.3. Primary Production

Daily (dawn-to-dawn, 24 h) rates of primary production were determined following the methodology of *Balch et al*. [2000]. Four replicate water samples (70 mL, 3 lights, 1 formalin-killed) were collected at a depth approximating the middle of the mixed layer (10–25 m, Table 2), spiked with 30–40 μCi of ^{14}C-labeled sodium bicarbonate and incubated on deck at 40% of incident irradiance following the incubator setup described in *Poulton et al*. [2010]. Incubations were terminated by filtration through 25-mm 0.4-μm Nuclepore polycarbonate filters, with extensive rinsing with fresh filtered seawater to remove any labeled ^{14}C-DIC, and filters were placed in 20 mL glass vials, with organic (PP) and inorganic (CP) carbon fixation determined using the Micro-Diffusion technique [*Poulton et al*., 2014]. Ultima-Gold liquid scintillation cocktail was added to the vials and activity on the filters was then determined on a Tri-Carb 2100 low-level liquid scintillation counter, with counts converted to uptake rates using standard methodology. The ^{14}C counts from the formalin-killed samples were subtracted from the light bottles.

Single depth measurements of PP were scaled to Ez integrals by accounting for both variability in the depth distribution of biomass (Chl-*a*) and the vertical attenuation of irradiance. Subsurface chlorophyll maxima (SCM) are known to represent important sources of PP in the Arctic Ocean [*Hill et al*., 2013] and irradiance also exerts a strong control on the vertical distribution of PP. Ez depths were identified as the depth of penetration of 1% of surface irradiance based on a biospherical 2π Photosynthetically Available Radiation (PAR)

Table 1. Biomass and Dominant Phytoplankton Species (or Genus) at Stations Sampled in the Mixed Layer During This Study[a]

Station	Date	Lat	Lon	Sampling Depth (m)	ML Depth (m)	Ez Depth (m)	Depth of the SCM (if Present) (m)	Chlorophyll-*a* (mg m^{-3})	Estimated C Phytoplankton (mmol C m^{-3})	Phytoplankton Biomass (mmol C m^{-3})			
										Diatom	*Phaeocystis*	Coccolithophores	Dominant Species
9	Jun 12 2012	74.1	−4.1	15	15	60	28	0.7	2.9	0.2		<0.1	*Thalassiosira* spp.
10	Jun 13 2012	76.1	−2.3	20	28	67	42	0.9	3.8	0.3		<0.1	Mixed diatoms
11	Jun 14 2012	78.4	0	10	20	21	10	8.4	35.0	0.2	31.3		*Phaeocystis pouchetii**
14	Jun 16 2012	77.5	1.1	10	70	63	23 (61)	0.1	0.4	<0.1	<0.1		*Thalassiosira* spp.
19	Jun 19 2012	71.7	17.9	16	15	28	14	3.5	14.6	0.3	4.6	<0.1	*Phaeocystis pouchetii*
26	Jun 22 2012	71.4	8.3	20	47	39		1.8	7.5	<0.1		0.1	*E. huxleyi*
32	Jun 25 2012	68.4	−10.3	13	15	62	12	1.1	4.6	0.3		<0.1	*Thalassiosira* spp.
34	Jun 26 2012	67.5	−16.2	15	18	32		2.1	8.8	0.2		0.3	*E. huxleyi*
36	Jun 27 2012	71.4	−1.2	20	35	38	35	1.9	7.9	21.8	0.1	0.2	*Ephemera* sp.*
38	Jun 28 2012	71.4	−10.3	25	10	55	32	0.5	2.1	0.3		0.1	Mixed diatoms
40	Jun 29 2012	68.4	−10.3	20	20	43	30	3.6	15.0	50.9		0.4	*Ephemera* sp.*
42	Jun 30 2012	67.5	−16.3	20	15	48	33	0.7	2.9	0.1	<0.1	<0.1	*Thalassiosira* spp.

[a]Note station 44 was not sampled for phytoplankton community structure. *E. huxleyi* stands for *Emiliania huxleyi*. Asterisks are mono-specific blooms. ML stands for mixed layer, Ez for euphotic zone, and SCM for subsurface chlorophyll maximum.

Table 2. Discrete Primary Production (mmol C m^{-3} d^{-1}) and Euphotic Zone Integrated Primary Production (mmol C m^{-2} d^{-1})[a]

Station	Sampling Depth (m)	Discrete Primary Production (mmol C m^{-3} d^{-1})	Integrated Primary Production (mmol C m^{-2} d^{-1})
9	15	0.9 ± 0.1	11.3 ± 0.8
10	20	2.2 ± 0.1	32.4 ± 1.2
11[b]	10	10.5 ± 2.1	58.9 ± 1.9
14[c]	10	0.8 ± 0.5	20.6 ± 12.4
19	16	5.2 ± 0.5	46.7 ± 5.0
26	20	1.8 ± 0.4	26.7 ± 5.3
32	13	1.5 ± 0.2	23.3 ± 2.9
34	15	2.3 ± 1.2	42.5 ± 21.6
36	20	3.9 ± 0.2	63.5 ± 3.9
38	25	1.1 ± 0.1	15.1 ± 1.3
40	20	1.6 ± 0.3	47.5 ± 8.1
42	20	1.3 ± 0.1	53.1 ± 6.0

[a]Note station 44 was not sampled for primary production.
[b]Station 11 was sampled at the ice edge (see section 3.1).
[c]Station 14 was sampled in the ice (see section 3.1) and integrated PP may be overestimated in this case due to the deep Ez (see Table 1).

sensor (Chelsea Technology Group Ltd) mounted on the CTD. The vertical diffuse attenuation coefficient of PAR (K_d) was then calculated based on the Ez depth. To integrate PP, we calculated the chlorophyll-specific rate of primary production (P^B; mg C (mg chl)$^{-1}$ d^{-1}) and used the calibrated fluorometer Chl-*a* profiles to estimate PP through the water column to the base of the Ez. Acknowledging that light availability will exert a strong vertical control on PP, we then used the K_d value to scale PP through the Ez and integrated these PP rates.

This method of estimating integrated PP assumes that phytoplankton photophysiology (e.g., P^B) is invariant with depth. If the phytoplankton community did show photophysiological variability with depth, for example, in an SCM, then our integration method would underestimate PP. However, as we did not make measurements of such physiological variability we are more confident in underestimating PP, although the potential effect on *ThE*-ratios should be noted (i.e., overestimates of *ThE*-ratio). A clear case where such physiological differences may be leading to an overestimate of Ez PP is station 14, where a deep Ez (70 m) is compensated by several SCM (Figure 2), leading to a high Ez PP relative to low rates of discrete PP at the sampling depth (Table 3). Hence, extrapolation of *ThE*-ratios should be treated with caution for this station.

2.4. Bacterioplankton and Protist Concentrations and Microbial Metabolic Activity

Concentrations of bacterioplankton and aplastidic protists were determined using flow cytometry. Seawater subsamples of 1.6 mL were preserved with paraformaldehyde (PFA, 1% final concentration) in 2 mL polypropylene screw cap vials. The vials were then placed in a fridge and left for no longer than 12 h. Samples were stained with SYBR Green I nucleic acid dye and analyzed using a FACSort flow cytometer (BD, Oxford) with internal bead standards [*Zubkov and Burkill*, 2006; *Zubkov and Tarran*, 2008].

Bacterioplankton production was estimated as the microbial uptake rate of Leucine using ^{14}C-Leucine (Hartmann Analytic, Germany), added at a concentration of 20 nM, in samples from different depths from each morning CTD. Subsamples of 1.6 mL from each sample were dispensed into 2 mL polypropylene screw cap vials containing ^{14}C-Leucine [*Zubkov et al*., 2000]. Samples were fixed at each time point (20, 40, 60, and 80 min) by the addition of 80 μL 20% PFA (1% v/w final concentration). Fixed samples were filtered onto 0.2 μm polycarbonate membrane filters soaked in nonlabeled Leucine solution to reduce adsorption of radiotracer. Filtered samples were washed twice with 4 mL deionized water. Radioactivity of samples was measured as counts per minute (CPM) by liquid scintillation counting (Tri-Carb 3100, Perkin Elmer, UK). Microbial uptake of Leucine was computed using specific activity of the Leucine radiotracer.

2.5. Carbon Export

Carbon export fluxes were calculated using the ^{234}Th "small-volume" technique with ICP-MS assessment of recoveries for ^{234}Th extraction [*Pike et al*., 2005]. Water samples were collected using GO-Flo bottles at 6–8 different depths within the upper 500 m with refined resolution in the top 150 m (Figure 2). All samples were checked for recovery of ^{234}Th extraction (90.3 ± 7.6%).Vertical profiles of ^{234}Th activity were converted to estimates of downward ^{234}Th flux using a one-dimensional steady state model [*Buesseler et al*., 1992] integrated to the depth of 100 m [*Cai et al*., 2010; *Chen et al*., 2003] as Ez integration [*Buesseler and Boyd*, 2009] was not suitable here. This is because at several stations the Ez was deeper than the depth of the mixed layer (Table 1 and Figure 2). We therefore report our export efficiency (see section 1) as *ThE*-ratios [*Buesseler*, 1998] and not Ez-ratios [*Buesseler and Boyd*, 2009]. We ignored the effect of horizontal and vertical advection and diffusion as these have been deemed to be insignificant in previous Arctic studies [*Cai et al*., 2010].

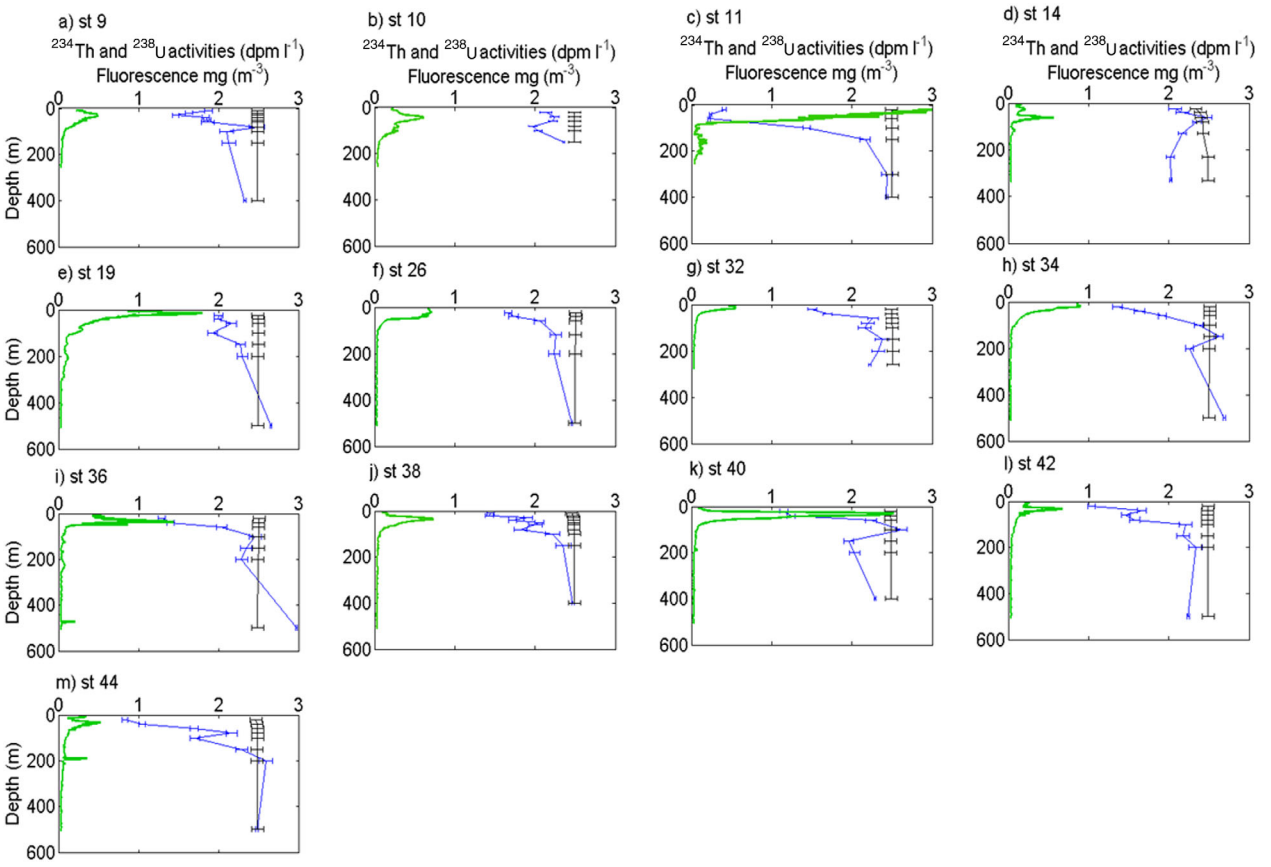

Figure 2. Vertical profiles of ^{234}Th and ^{238}U activity (dpm L^{-1}) and fluorescence (mg m^{-3}) during JR 271. Station numbers are indicated.

We did not use the nonsteady state approach as it only improves the flux estimates in cases where the sampling was conducted in a Lagrangian framework [*Resplandy et al.*, 2012] which was not possible during this cruise. A triplicate of deep water (2000 m) samples was collected at station 9 in order to verify the calibration of the method. Averaged ^{234}Th:^{238}U ratio was 0.98 ± 0.02 (n = 3). The ^{238}U activity was determined by using the ^{238}U-salinity relationship described in *Chen et al.* [1986].

Table 3. Thorium Flux (dpm m^{-2} d^{-1}) Integrated at 100 m (See Section 2), C:Th Ratio (μmol dpm^{-1}), C:Th Ratio Sampling Depth (m), POC Export (mmol m^{-2} d^{-1}) From the ^{234}Th Technique During JR271[a]

Station	Thorium Export (dpm m^{-2} d^{-1})	C:Th Ratio (μmol dpm^{-1})	C:Th Ratio Sampling Depth (m)	POC Export (^{234}Th) (mmol m^{-2} d^{-1})	*ThE*-Ratio
9	1342 ± 382	4.6 ± 0.5	50	6.2 ± 1.9	0.5 ± 0.2
10	862 ± 204	4.0 ± 0.4	40	3.4 ± 0.9	0.10 ± 0.03
11	4324 ± 164	18.1 ± 1.9	30	78.3 ± 8.7	1.3 ± 0.3
14	143 ± 212	12.8 ± 1.8	80	1.8 ± 3.8	0.09 ± 0.2
19	948 ± 208	9.4 ± 0.9	50	8.9 ± 2.1	0.19 ± 0.05
26	1267 ± 215	11.5 ± 1.5	60	14.6 ± 3.1	0.5 ± 0.2
32	1125 ± 326	5.0 ± 0.5	30	5.7 ± 1.7	0.2 ± 0.1
34	1374 ± 199	4.2 ± 0.5	30	5.8 ± 1.1	0.1 ± 0.1
36	1367 ± 205	5.0 ± 0.5	50	6.8 ± 1.2	0.11 ± 0.02
38	1576 ± 374	4.1 ± 0.5	60	6.4 ± 1.7	0.4 ± 0.1
40	1187 ± 206	10.8 ± 1.3	60	12.8 ± 2.7	0.3 ± 0.1
42	2023 ± 302	8.6 ± 1.0	60	17.4 ± 3.3	0.3 ± 0.1
44	2105 ± 303	9.0 ± 0.9	50	18.9 ± 3.4	

[a]*ThE*-ratio is also presented.

These fluxes were then converted to estimates of downward organic carbon flux using the C:Th ratio in large (>53 μm) particles collected using an in situ Stand Alone Pumping System (SAPS) deployed for 1.5 h at a single depth beneath the mixed layer (depths given in Table 3). Particles were then rinsed off the screen using particulate thorium-free seawater (obtained from seawater filtered through a 0.4 μm polycarbonate filter), and the particle suspension evenly split into subsamples using a Folsom splitter. Splits were then analyzed for ^{234}Th and POC as described in *Le Moigne et al*. [2013b], with no replicates analyzed. Particulate ^{234}Th and C samples were analyzed from two distinct splits. POC flux at from the base of the mixed layer [*Smith*, 2014] (Table 1 and supporting information Table S1) was measured using the Marine Snow Catcher following methods described in *Cavan et al*. [2015] and *Riley et al*. [2012].

2.6. Zooplankton Respiration Rate

Zooplankton community respiration rates were estimated from determination of the composition and abundance of the biomass-dominant species at each locality, subsequently converted to respiration rates as a function of species-weight and in situ sea surface temperature from the ship's underway system. Zooplankton were sampled between 0 and 200 m with a motion compensated Bongo net following sampling procedures described in *Ward et al*. [2012]. Specific respiration rate (μl O_2 ind^{-1} h^{-1}) of each biomass-dominant species at each station was determined from relationships detailed in *Ikeda et al*. [2001] through applying values for in situ temperature and species dry weight (supporting information Table S2) as described in equation (1):

$$\text{Specific respiration rate} = e^{(-0.399+(0.801\times(\ln DW)))}+(0.069\times SST) \quad (1)$$

where *DW* is the dry weight of each individual species and stage (in mg) and *SST* is the sea surface temperature from the ship's underway system (in °C). Species respiration rate (μl O_2 ind^{-1} h^{-1}) was multiplied by species abundance (individuals m^{-2}) and then summed across all biomass-dominant species to determine community respiration rate (μl O_2 m^{-2} h^{-1}) at each station as in equation (2):

$$\text{community respiration rate} = \sum \text{Specific respiration rate} \times Abundance_{int} \quad (2)$$

where $Abundance_{int}$ is the integrated abundance of each species and stage over the top 200 m of the water column. We were not able to determine levels of error around our estimates of zooplankton community respiration since they are based on an extrapolation of the function developed by *Ikeda et al*. [2001] on temperature and weight specific zooplankton community respiration.

3. Results

3.1. General Hydrography

We sampled a large mix of oceanic habitats, including open water, ice-edge, and ice-covered waters (Figure 1a). In the Barents Sea (Stn. 32) and Norwegian Sea (Stns. 26, 34, and 36), surface waters were warmer than in the Greenland Sea (Stns. 9, 10, 38, 40, 42, and 44) reflecting the influence of Atlantic waters flowing northward. The Greenland Sea was under the influence of southward flowing polar waters. Three stations across the Fram Strait in close proximity to one another typified the local gradient in sea ice conditions, from under ice (more than 90% ice concentration, Stn. 14), ice-edge (Stn. 11) to ice-free waters (Stn. 19) (Figure 1a and supporting information Figure S1), with the ice station displaying a clear input of fresh water at the surface (supporting information Figures S2 and S3).

3.2. Chlorophyll, Primary Production, and Phytoplankton Composition

Chl-*a* concentration in the middle of the mixed layer (see sampling depth in Table 1) ranged from 0.1 to about 8.5 mg m^{-3} (Figure 1b). The full CTD calibrated fluorescence Chl-*a* is presented in Figure 2. The ice station (Stn. 14) had the lowest concentration (0.1 mg m^{-3}) while the two nearby stations (Stns. 11 and 19) had the highest (8.5 and 3.5 mg m^{-3}, respectively). Elsewhere, there was a clear divide between the Greenland Sea (average Chl-$a = 0.54 \pm 0.1$ mg m^{-3}) and the Norwegian/Barents Seas (average Chl-$a = 1.7 \pm 0.4$ mg m^{-3}). These trends were also true for mixed layer Chl-*a* concentrations (Table 1).

Clear subsurface chlorophyll maxima (SCM) were observed in the Greenland Sea (Figure 2). However, in the Barents/Norwegians Seas, vertical fluorescence profiles show that Chl-*a* concentrations were high within the mixed layer and decrease quasi-exponentially below it. At most stations, the Ez depth was deeper than

the mixed layer depth (MLD) (Table 1), apart from at station 26. The presence of an SCM was clear at stations 9, 10, 14, 36, 38, 40, and 42 (Figure 2 and Table 1). SCM were generally located between the MLD and the Ez depth, with the exception of stations 14 and 36 where SCM, MLD, and Ez depths were all very close to each other (Table 1 and Figure 2).

The sampling depth for PP and phytoplankton composition ranged from 10 to 25 m rather than surface waters (i.e., <5 m), and was in most cases close to the depth of SCM or within 10–20 m of it (Table 1). For all but four of the sampling stations (Stns. 9, 10, 38, and 40), the SCM and sampling depth were shallower or near to the mixed layer depth, and hence we can have confidence that in most cases upper mixed layer (where we sampled PP and community structure) is representative of SCM (where a significant fraction of export can occur). Importantly, none of the key stations for our conclusions (Stns. 11, 14, and 19) suffer from significant differences in depths between sampling, SCM, and MLD.

Unlike Chl-*a*, integrated PP rates (Table 2) did not display any clear geographical pattern although the lowest PP was recorded at the ice stations (Figure 1a; Stn. 14, 20.6 ± 12.4 mmol C m^{-2} d^{-1}) and the highest PP was recorded at the boundary between the Norwegian and Greenland Seas (Stn. 36, 63.5 ± 3.9 mmol C m^{-2} d^{-1}) (Table 2). Other stations like station 11 (58.9 ± 11.8 mmol C m^{-2} d^{-1}) located at the ice edge (Figure 1a) and station 42 (53.1 ± 6.0 mmol C m^{-2} d^{-1}) located near Iceland, also had relatively high PP rates.

Three distinct plankton groups were dominant in the survey area during June 2012. Diatoms dominated the phytoplankton community at most of the open ocean stations with genera like *Thalassiosira* and *Ephemera* present (Table 1). At stations where *Ephemera* was observed, this species represented more than 90% of the total phytoplankton biomass (Table 1). The coccolithophore *Emiliania huxleyi* was observed in the Norwegian and the Barents Seas, as commonly observed in this region [*Smyth et al*., 2004]. In the high Chl-*a* area observed at the ice edge (Stns. 11 and 19, Figure 1), the colonial haptophyte *Phaeocystis pouchetii* was the major species in terms of biomass (Table 1). At station 11, *P. pouchetii* cells represented more than 90% of the phytoplankton carbon, while at station 19 the dominance of this species was much less pronounced (~30% of phytoplankton carbon, Table 1). In the ice covered region, diatoms and coccolithophores were observed but in small abundances which accounted for little biomass (Table 1).

3.3. POC Export Fluxes

3.3.1. ^{234}Th Activity Profiles and Integrated Fluxes

Vertical profiles of ^{234}Th and ^{238}U activities are presented alongside Chl-*a* fluorescence profiles in Figure 2. The lowest ^{234}Th activities (0.3–1 dpm L^{-1}) were observed in subsurface waters at station 11 and also in the Greenland Sea, near Iceland (Stns. 40, 42, and 44) suggesting a large removal of sinking particles at this stations. The highest ^{234}Th activity (3 dpm L^{-1}) was found at 500 m at station 36. While at this depth, the ^{234}Th is expected to be at equilibrium with the ^{238}U, this high value may reflect localized particle fragmentation (which does not necessarily means remineralization).

The most striking result is the ^{234}Th profile at station 14 (in ice) where the surface (0–60 m) ^{234}Th activities were low, and reach equilibrium approximately at the depth of the SCM (Table 1), though they decrease again below it. It is difficult to say whether this is due to particle export occurring deeper in the water column or some other process. Also, the ^{238}U activity at this station may not be accurate as the ^{238}U to salinity relationship we used here [*Chen et al*., 1986] does not cover the salinity range encountered at this station (32–35 for this station; see supporting information Figure S3 and 34.5–35.5 in *Chen et al*. [1986]). *Lalande et al*. [2008] observed a similar feature in the Barents Sea. This has, however, only a limited effect on the ^{234}Th fluxes as it occurs further down the water column relative to the depth the ^{234}Th fluxes were integrated to (i.e., 100 m).

The steady state 100 m integrated flux of ^{234}Th (see section 2) was large at station 11 and stations 42–44 (2023 ± 302–4324 ± 164 dpm m^{-2} d^{-1}) indicating one of the largest export of particles recorded worldwide [*Le Moigne et al*., 2013a]. At other stations, the deficits were moderate (from 862 ± 204 to 1576 ± 374 dpm m^{-2} d^{-1}) or low (e.g., Stn. 14, 143 ± 212 dpm m^{-2} d^{-1}) (Table 3). Previous ^{234}Th deficits (integrated to a similar horizon depth as in this study) measured within *Phaeocystis* sp. blooms in the Arctic are consistent with our results [*Lalande et al*., 2007, 2008]. Furthermore, deficits recorded at stations 34, 36, 38, 40, and 42 are also consistent with previous ^{234}Th deficits in the presence of similar phytoplankton community structure ([*Martin et al*., 2011], 2200 dpm m^{-2} d^{-1}, diatom bloom) ([*Sanders et al*., 2010], 987–2700 dpm m^{-2}

d^{-1}, coccolithophore rich waters). Under the ice, at station 14, the ^{234}Th deficit was low (143 ± 212 dpm m^{-2} d^{-1}) (Table 3) consistent with other under ice studies [*Cai et al*., 2010; *Chen et al*., 2003].

3.3.2. C:Th Ratios and POC Export Fluxes

^{234}Th fluxes were converted to estimates of downward particle flux using the POC:^{234}Th ratio (hereafter abbreviated as C:Th) in large (>53 μm) particles [*Buesseler et al*., 1992] (Table 3). C:Th ranged from 4 to 18 μmol C dpm^{-1}. The largest C:Th ratios were observed in the ice–edge and under the ice (Stns. 11 and 14), near the Barents Sea (Stn. 26) as well as in the southern sector of the Greenland Sea (Stns. 40–44) (Table 3).

Generally, POC export fluxes displayed a trend of decreasing flux from south to north with relatively large fluxes (12.8 ± 2.7–18.9 ± 3.4 mmol C m^{-2} d^{-1}) at stations close to Iceland (Stns. 40, 42, and 44) and low fluxes (1.8 ± 3.8–6.2 ± 1.97 mmol C m^{-2} d^{-1}) in the northernmost part of the survey and the Barents Sea (5.7 ± 1.7 mmol C m^{-2} d^{-1}). The under ice station (Stn. 14) had the lowest flux (1.8 ± 3.8 mmol C m^{-2} d^{-1}) (Table 3). An exception to this geographical pattern was station 11, located at the ice edge (Figure 1a) where the POC fluxes was surprisingly high (78.3 ± 8.7 mmol C m^{-2} d^{-1}) (Table 3).

4. Discussion

4.1. POC Export

There are only a few studies that have looked at the export of carbon in the Atlantic sector of the Arctic Ocean [*Le Moigne et al*., 2013a]. Most of the effort in this sector of the Arctic Ocean has previously been concentrated on the shallow waters of the Barents Sea [*Coppola et al*., 2002; *Lalande et al*., 2008] and the ice covered Fram Strait [*Rutgers van der Loeff et al*., 2002]. Our data are thus unique for the Arctic, and are likely more comparable to what has been found in other deep-sea high latitude "ice-free" regions as described in section 3.3.1. POC export flux at station 32 in the Barents Sea (5.7 ± 1.7 mmol C m^{-2} d^{-1}, Table 3) was on the lower range of what has been found previously [*Coppola et al*., 2002; *Lalande et al*., 2008]. In the open waters of Greenland and Norwegian Seas (Stns. 9, 10, 26, and 34–44), POC export flux ranged from 3.4 ± 0.9 to 18.9 ± 3.4 mmol C m^{-2} d^{-1} (Table 3). To our knowledge, this is the first attempt to measure the export of POC in this region [*Le Moigne et al*., 2013a], which makes comparison with POC fluxes from other oceanographic environments difficult. In the Fram Strait (Stns. 11–19), POC export flux showed the largest variability due to the presence of sea ice, ice-edge, and ice-free conditions. POC export fluxes in the Fram Strait (Table 3) are consistent with previous measurements over an ice covered/ice-free gradient in the Arctic [*Cai et al*., 2010]. Station 11 located at the ice edge, however, displayed a surprisingly high POC export flux (78.3 ± 8.7 mmol C m^{-2} d^{-1}), potentially due to the presence of a *P. pouchetii* bloom (Table 1 and Figure 1b).

C:Th ratios in blooms of *Phaeocystis* measured using large volume filtration units (as in our study) have previously been deemed to be overestimated relative to C:Th ratios measured in sediment traps due to the large proportion of dissolved organic carbon or mucilage released by *Phaeocystis* [*Lalande et al*., 2008]. C:Th measured in *Phaeocystis* blooms at different stages in the Barents Sea [*Lalande et al*., 2008, Table 3] with pumps were much higher (49 ± 48 μmol dpm^{-1}) than those measured with traps (10 ± 4 μmol dpm^{-1}), with the traps considered as providing more accurate C:Th ratio measurements. The authors [*Lalande et al*., 2008] concluded that the carbon mucilage released by blooming *Phaeocystis* may yield inaccurate (overestimated) C:Th ratios if collected using pumps. However, the C:Th measured at station 11 using pumps in our study (18 μmol dpm^{-1}) was almost identical to the value of *Lalande et al*. [2008] (16 μmol dpm^{-1}) in an ongoing *Phaeocystis* bloom. Hence, we are confident in our pump-derived C:Th ratio for this station where the *Phaeocystis* bloom was observed (Stn. 11). The high POC flux at station 11 was not only recorded by the ^{234}Th technique, but also using the Marine Snow Catcher (a modified settling chamber for instantaneous flux estimates) [*Cavan et al*., 2015; *Riley et al*., 2012], with full description in *Smith* [2014] (supporting information Table S1).

The instantaneous POC flux measured at 30 m (10 m below the MLD) using the Marine Snow Catcher yielded a flux of 156 ± 51 mmol C m^{-2} d^{-1} for station 11 (supporting information Table S1) [*Smith*, 2014], which is roughly twice the value measured from ^{234}Th (78.3 ± 8.7 mmol C m^{-2} d^{-1}). For comparison, the average POC flux measured by the Marine Snow Catcher at similar depths across all the sampling sites was 32 ± 16 mmol C m^{-2} d^{-1} (compared to 8 ± 9 mmol C m^{-2} d^{-1} for the ^{234}Th-derived flux). The Marine Snow Catcher-derived POC fluxes are generally larger than the ^{234}Th-derived POC fluxes due to the

Table 4. Dominant Phytoplankton Community Structure (PCS) in Terms of Biomass (See Supporting Information Table S1), Euphotic Zone Integrated Primary Production, Carbon Export, and the Calculated Export Efficiency

Dominant PCS and Ice Conditions[a]	Station	Integrated Primary Production (mmol C m^{-2} d^{-1})[b]	C Export (mmol C m^{-2} d^{-1})[c]	*ThE*-ratio
Phaeocystis sp. (ice edge)	11, 19	46.7 ± 5.0–58.9 ± 1.9	8.9 ± 2.1–78.3 ± 8.7	0.19 ± 0.05–1.3 ± 0.3
Ice	14	20.6 ± 12.4	1.8 ± 3.8	0.09 ± 0.19
Coccolithophores (open)	26, 34	26.7 ± 5.3–42.5 ± 21.6	5.8 ± 1.1–14.6 ± 3.1	0.1 ± 0.1–0.5 ± 0.2
Diatoms (open)	9, 10, 32, 36, 38, 40, 42	11.3 ± 0.8–63.5 ± 3.9	3.4 ± 0.9–17.4 ± 3.3	0.10 ± 0.03–0.5 ± 0.2

[a]See Table 1.
[b]See Table 2.
[c]See Table 3.

fundamental difference in the time scale over which both approaches integrate the POC export fluxes and the export horizon considered for both approaches.

For instance, we know that in postbloom conditions, ^{234}Th-derived POC export is likely to overestimate the actual POC export relative to free-drifting sediment traps deployed for a couple of days [*Le Moigne et al*., 2013b]. In developing bloom conditions, like at some of the stations sampled in our study (e.g., Stn. 9, for example), it is possible that this discrepancy is limited. As mentioned above, the MSC flux at station 11 clearly stands out relative to the other stations. We therefore believe that both our ^{234}Th flux and C:Th ratio provide accurate measurements leading to the robust estimation of carbon export at station 11 (see data presented in supporting information Table S1).

4.2. Export Efficiency and Phytoplankton Community Composition

Overall, *ThE*-ratios ranged from 0.09 ± 0.19 to 1.3 ± 0.3 (Figure 3, Tables 3 and 4), which is similar to the range seen in open waters elsewhere [*Buesseler*, 1998; *Buesseler and Boyd*, 2009]. Only station 11 stands out as having a particularly high value (1.3 ± 0.3). The three stations located in the Fram Strait are of a particular interest since, although levels of PP are similar (20.6 ± 12.4–58.9 ± 1.9 mmol C m^{-2} d^{-1}, Table 2, variance = 117), ^{234}Th-derived carbon export fluxes were relatively variable (1.8 ± 3.8–78 ± 8.7 mmol C m^{-2} d^{-1}, Table 3, variance = 1191), displaying higher variability than PP. This equates to *ThE*-ratios ranging from 0.09 ± 0.19 to 0.19 ± 0.05 under ice (Stn. 14) and in ice-free conditions (Stn. 19) to as high as 1.3 ± 0.3 at the ice edge (Stn. 11). Such a high *ThE*-ratio at the ice edge implies that a substantial fraction of PP was exported out of the Ez. In the Barents Sea (Stn. 32) by comparison, the *ThE*-ratio was moderate (0.2 ± 0.1). *ThE*-ratios ranged from 0.1 ± 0.0 to 0.5 ± 0.2 in the Greenland and Norwegian Seas (excluding stations in the Fram Strait). Station 10 also stood out because of its lower *ThE*-ratio (0.10 ± 0.03), while consistently high *ThE*-ratios (0.3 ± 0.1–0.4 ± 0.1) were observed at stations located north of Iceland (Stns. 9, 38, 40, and 42).

On the global scale, phytoplankton community structure has been suggested to influence BCP efficiency [*François et al*., 2002], for example, through the supply of dense material, such as opal and calcite, to ballast sinking organic material. However, although global patterns of both *ThE*(Ez)-ratio [*Siegel et al*., 2014] and ballasted POC flux to a certain extent correlate [*Le Moigne et al*., 2014], other processes related to recycling and ecosystem structure may also greatly affect the *ThE*(Ez)-ratio [*Henson et al*., 2012; *Lam et al*., 2011; *Le Moigne et al*., 2014]. Therefore, whether there is a strong relationship between phytoplankton composition and *ThE*-ratios in the Arctic Ocean is very much an open question. We now examine *ThE*-ratios produced by the various phytoplankton groups we observed (Table 1) at each station undergoing a phytoplankton bloom (elevated biomass).

At high latitudes, the POC *ThE*-ratio can vary seasonally [*Baumann et al*., 2013; *Buesseler et al*., 1992; *Kawakami et al*., 2007] to a greater extent than at low latitudes [*Benitez-Nelson et al*., 2001; *Brix et al*., 2006; *Buesseler et al*., 1995]. A recent modeling study confirmed that, in prebloom conditions, the *ThE*-ratio is low and then increases during the bloom to reach its pinnacle in postbloom conditions [*Henson et al*., 2015]. Therefore, to truly compare the effect of phytoplankton community structure on the *ThE*-ratio, one must compare stations where different phytoplankton communities are growing, at a similar point in their seasonal bloom cycle (e.g., sampled during prebloom, bloom, or postbloom conditions).

Figure 4 shows the time series of MODIS satellite-derived Chl-*a* (averaged over 100 × 100 km with 8 day resolution) for each station. We assume here that the blooming conditions correspond to the highest Chl-*a*

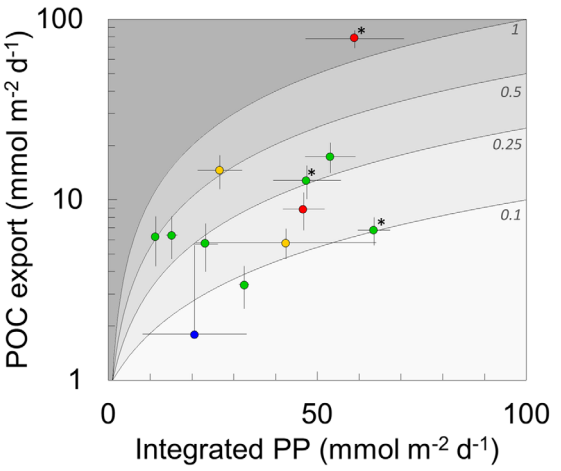

Figure 3. Euphotic zone integrated carbon export flux and primary production. Stations are colored according to the microphytoplankton functional type characterizing the community structure (green = diatom dominated stations, yellow = stations with coccolithophores present, red = *Phaeocystis pouchetii* dominated stations, and blue = under ice station). Stars indicate stations where the dominant phytoplankton type represented more than 90% of the microphytoplankton biomass. Error bars indicate standard deviation performed on replicates for integrated PP and the propagated analytical error for the POC export obtained from the ^{234}Th technique. *ThE*-ratio values [*Buesseler*, 1998] are indicated and shaded. See Tables 2 and 3.

satellite concentration recorded during the year. Stations 9, 10, and 19 were considered to be in a prebloom state (Figure 4). Although at stations 10 and 19, the PP was already high (Figure 1 and Table 2) suggesting that they were in an ascending bloom regime, Chl-*a* concentration had not yet reached its maximum. Export fluxes (Figure 1d) as well as *ThE*-ratios (0.10 ± 0.03–0.2 ± 0.0) (Figure 2) were consistently low at these stations. Conversely, stations 11, 26, 32, 34, 36, 38, 40, and 42 were sampled either at the beginning or during the main peak of bloom or shortly (less than a month) after the peak of it (Figure 4). At these stations, *ThE*-ratios ranged from 0.11 ± 0.02 to 1.3 ± 0.3. We hereafter refer to these stations as blooming stations. We cannot assess the bloom situation at station 14 (under ice) as no satellite Chl-*a* data were available at this station due to the presence of ice (Figure 1a).

Blooming stations near Iceland (Stns. 38, 40, and 42) were dominated by diatoms and had a consistently high *ThE*-ratio (0.3 ± 0.1–0.4 ± 0.1), comparable to previously reported values for a bloom in the North Atlantic [*Buesseler and Boyd*, 2009]. The blooms where *E. huxleyi* was present and comprised a

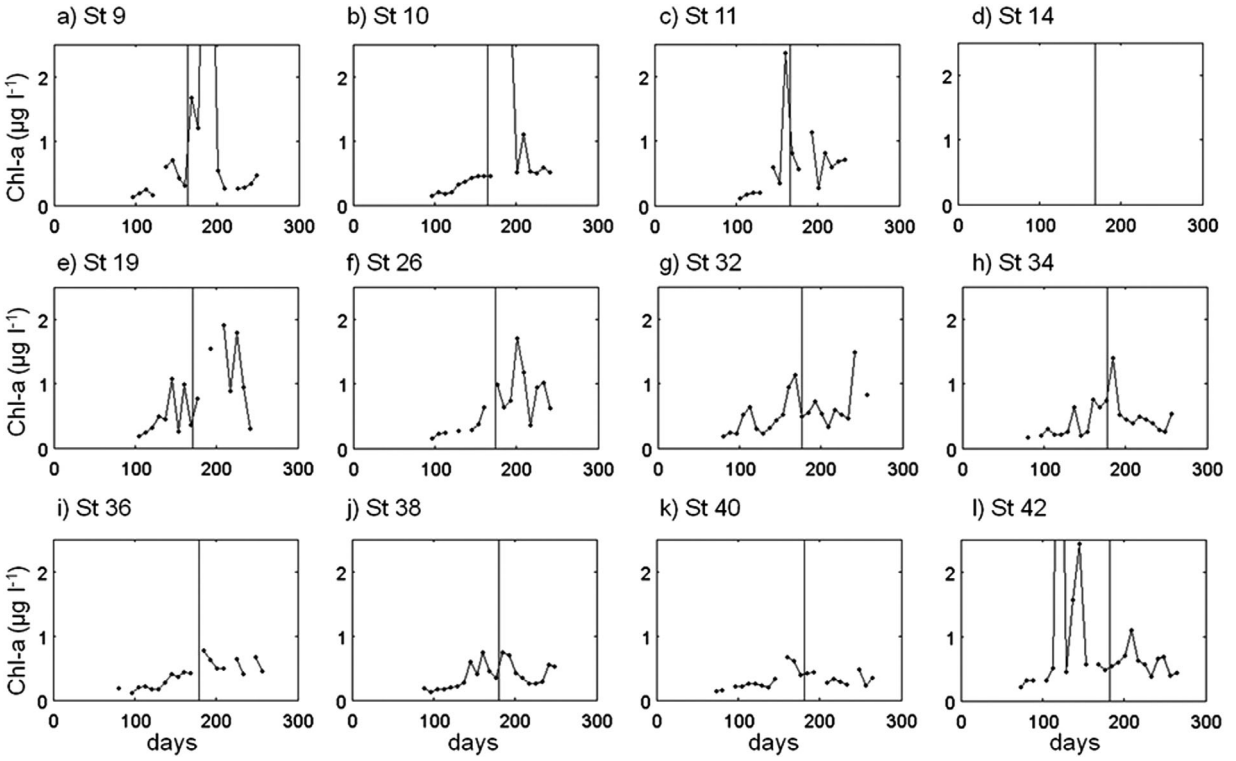

Figure 4. Time series of MODIS satellite Chl-*a* (averaged over a 100 × 100 km box centered on the station with 8 day temporal resolution) for each station. The blue vertical line represents the sampling date (note there is no satellite Chl-*a* data available for station 14 due to ice cover).

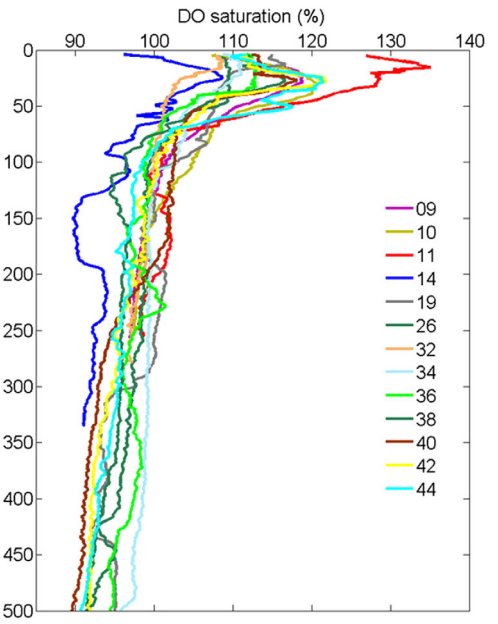

Figure 5. Dissolved oxygen (% saturation) at all stations (see section 4.1).

significant fraction of the biomass without being the dominant species (Table 1) also had a fairly high *ThE*-ratio (0.1 ± 0.1–0.5 ± 0.2) (Table 4). However, the highest *ThE*-ratio (1.3 ± 0.3) (Figure 3) found in our study area was associated with high biomass (8.5 mg Chl-*a* m^{-3}), high integrated PP (58.9 mmol C m^{-2} d^{-1}) and dominance (>90% of biomass, Table 1) of the phytoplankton community by the haptophyte *P. pouchetii*. *P. pouchetii* was also present at the open ocean station (Stn. 19), but here it was not a mono-specific bloom as observed at station 11 (Table 1). Also, station 19 had not yet reached peak bloom at the time of sampling as revealed by the satellite Chl-*a* time series (Figure 3e) and had a lower *ThE*-ratio (0.19 ± 0.05). In contrast to the ice-edge station, this open ocean site had lower biomass, lower PP, and lower *P. pouchetii* biomass (Figure 1 and Table 1). This station is in a typical prebloom state (e.g., a station where Chl-*a* and PP are increasing but export has yet to start, see Figures 1b, 1c, and 2) as described in *Henson et al.* [2015]. As expected from previous studies, the *ThE*-ratio was low (Figure 2) under the ice [*Cai et al.*, 2010].

Buesseler and Boyd [2009] reported high latitude *ThE*-ratios from the north Atlantic, the north Pacific, and the Southern Ocean, all largely dominated by diatoms. To our knowledge, we present the first estimate of *ThE*-ratios associated with polar blooms in which significant biomass was associated with coccolithophores and *Phaeocystis* sp. Export efficiency from such regions has been estimated before but with limited information on the community composition [*Cai et al.*, 2010; *Chen et al.*, 2003] or with an export efficiency calculation methodology different from the *ThE*-ratio approach [*Reigstad et al.*, 2008; *Smith et al.*, 1991] used here, and thus prevents any direct comparison. Previously, only diatom dominated blooms were thought capable

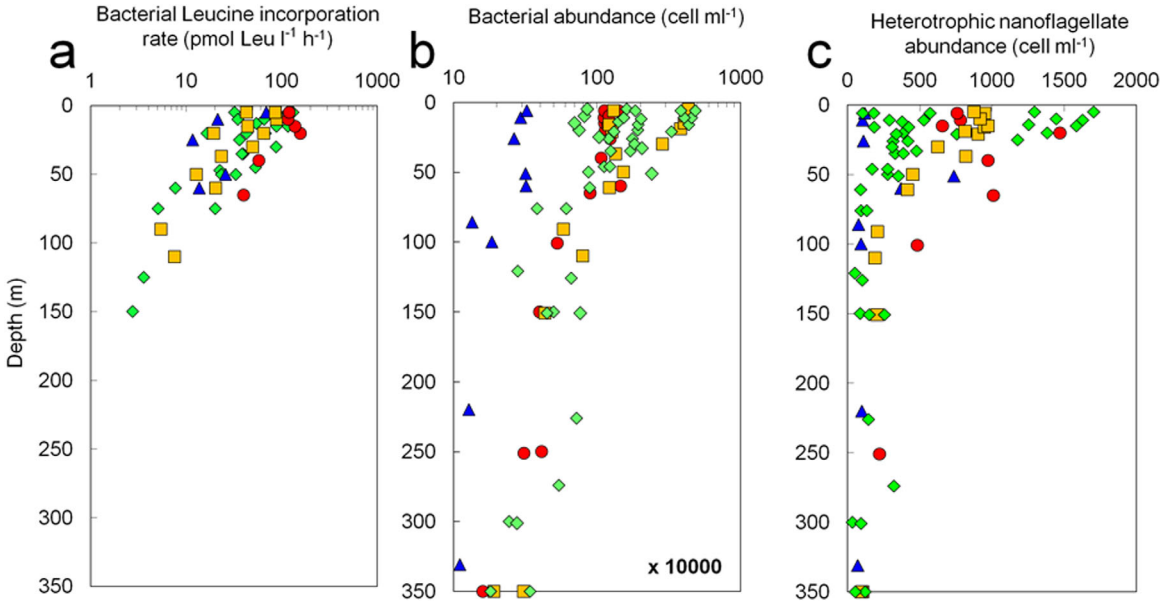

Figure 6. (a) Bacterial Leucine incorporation rate (pmol Leu L^{-1} h^{-1}). (b) Bacterial abundance (cell mL^{-1}). (c) Hetetrophic nanoflagellate abundance (cell mL^{-1}). Stations are colored according to the microphytoplankton functional type characterizing the community structure (green = diatom dominated stations, yellow = stations where coccolithophores were present, red = *Phaeocystis pouchetii* dominated stations, and blue = under ice station).

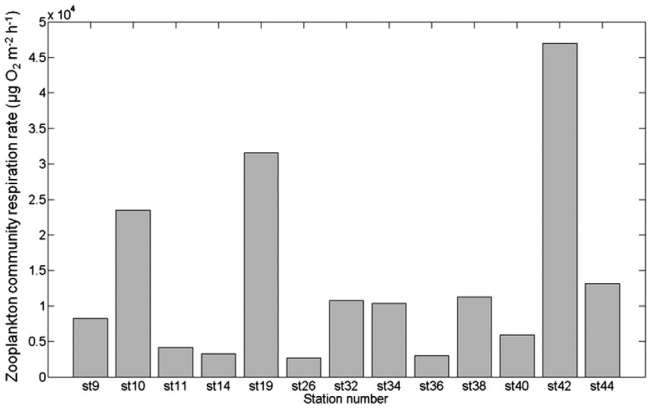

Figure 7. Zooplankton community respiration rate (µg O_2 L^{-1} h^{-1}) integrated over the top 200 m.

of producing high *ThE*-ratios with values reaching 0.45 during the diatom dominated North Atlantic bloom experiment [*Buesseler and Boyd*, 2009]. However, our observations from the ice edge of the Greenland Sea indicate that the presence of *P. pouchetii* can yield *ThE*-ratios at least as high as blooming diatoms [*Buesseler and Boyd*, 2009] (Figure 2 and Table 4).

4.3. Remineralization

Although we observed efficient export (i) in an ice edge associated *P. pouchetii* bloom (1.3 ± 0.3), (ii) where coccolithophores were present near the Barents Sea (0.1 ± 0.1–0.5 ± 0.2), and (iii) in diatom dominated conditions in the Greenland Sea near Iceland (0.3 ± 0.1–0.4 ± 0.1), this material may be highly remineralized just below the depth of the Ez and will not contribute greatly to long-term carbon sequestration. While a high *ThE*-ratio indicates that a significant portion of surface PP is exported out of the surface layer [*Buesseler*, 1998; *Buesseler and Boyd*, 2009], recent studies have suggested that significant remineralization within the upper part of the mesopelagic (<300 m depth) could prevent material from efficiently reaching deeper waters [*Buesseler and Boyd*, 2009; *Giering et al*., 2014] and thus contributing to C sequestration.

This hypothesis has not been examined previously in the Arctic. Hence, it has not previously been possible to assess the potential importance of Arctic blooms to the air-sea partitioning of atmospheric CO_2 in polar oceans. Here we do not attempt to estimate the T_{100} ratio [*Buesseler and Boyd*, 2009], as this metric requires two independent estimates of POC export flux: one below the Ez depth (which we have) (Figure 1d) and another 100 m below the Ez depth (which we do not have). This is because estimating POC flux using the ^{234}Th technique at 100 m below the Ez depth requires high resolution sampling in both the surface and deeper in the upper mesopelagic [*Buesseler and Boyd*, 2009], which was not possible during this cruise.

Instead, to examine whether substantially more remineralization (>100 m) of carbon occurred at certain stations relative to others, we compare several indirect but independent indicators of microbial activity rates. These are not actual carbon remineralization rates, but nevertheless provide relative information (integrated on various time scales) on the magnitude of the upper mesopelagic remineralization at each station. These include dissolved oxygen saturation ([DO] in %) (Figure 4), bacterial Leucine uptake, bacterial/heterotrophic flagellate abundance (Figure 5), and integrated zooplankton respiration rate (Figure 6).

We acknowledge that all these estimates and indicators integrate remineralization processes over different time scales. For instance, the bacterial Leucine uptake and the integrated zooplankton respiration rates look at instantaneous remineralization while the [DO] gives information on the seasonal time scale (several months). This has the great advantage in that encompasses the time scale over which our *ThE*-ratio (which couples monthly integrated estimates of POC export with instantaneous (daily) PP estimates) is integrated over.

4.3.1. Oxygen Saturation

Oxygen is produced during photosynthesis and consumed during the respiration (remineralization) of organic matter [*Koeve*, 2001]. Hence, in a water mass where the winter mixed layer is sufficiently deep that the water column is renewed at the end of the productive season, as in the Atlantic sector of the Arctic Ocean [*de Boyer Montegut et al*., 2004], vertical profiles show supersaturation of oxygen (>100%) in upper ocean productive waters and increasing under-saturation (<100%) with depth, due to the dominance of respiration over photosynthetic production [*Koeve*, 2001] (Figure 4a). This provides information on how large the upper mesopelagic respiration rate was from the end of the winter up to the sampling date. It is thus important at this stage to investigate whether the surface (surface to mixed layer depth) and subsurface water masses (mixed layer depth to 300 m) could potentially have a different origin and history,

especially in the Fram Strait where the hydrography is complex due to the narrow topography and the influence of various waters masses [*Woodgate*, 2013].

We found station 14 (under the ice, see Figure 1) to be clearly influenced by cold and/or less saline (salinity <34) fresh water from ice melt [*Woodgate*, 2013] in the surface. However, the density profiles and temperature/salinity diagram (supporting information Figures S3 and S4) at station 11 displays an homogeneous water mass within the upper 250 m (salinity $\sim$35; temperature 3–3.5°C) suggesting that the influence of Atlantic waters (salinity 34–5; temperature 0–2°C), occasionally observed in subsurface waters ($>$150 m) in the eastern sector of the Fram Strait [*Woodgate*, 2013] was limited at this station during our survey. Station 19 was influenced by fresher waters in the surface. Close to Svalbard, the surface waters may freshen slightly due to the nearby Barents Sea Polar Front separating the East Spitsbergen Current and West Spitsbergen Current, which is located approximately over the shelf break.

In the Greenland Sea (Stns. 9, 10, 38, 40, 42, and 44), the salinity and temperature range for this area are between 34.4–35 and -1.8–4°C, respectively [*Hopkins*, 1991]. There is a rather complex series of recirculation, atmospheric exchanges, interleaving, and mixing which gives rise to a broad variety of water masses in this region [*Rudels et al.*, 2005]. Surface waters at stations 9, 10, 40, 42, and 44 originate from a single water mass but station 38 displayed unique features (supporting information Figure S4). This station is clearly influenced by fresher and colder waters. This is likely due to the position of this station, which is located slightly west of the East Greenland Front where the influence of the southward flowing East Greenland current is stronger. The water the Norwegian and Barents Seas (Stns. 26, 32, 34, and 36) has a strong influence from the North Atlantic Water, and has been defined by *Loeng* [1991] as salinity greater than 35 and temperature from 3.5 to 6.5°C. The temperature salinity diagram shows water sampled at stations 26, 34, and 36 originated from a single water mass. However, as for station 38, station 32 seems influenced by two different water masses (Figure S4). The presence of a surface coastal current of similar temperature but lower salinity is a possibility in the Norwegian Sea where station 32 was located.

For blooming stations in our study area, surface supersaturation ($>$105%) is evident in the upper 50 m (Figure 4), with [DO] reaching as high as 135% at the site of the *P. pouchetii* bloom. At depths down to 250 m, [DO] remains $>$95% at diatom dominated stations similar to stations in the Barents Sea (Figure 4). Below the *P. pouchetii* bloom (Stn. 11), [DO] also remains $>$95% indicating relatively similar levels of respiration of sinking organic matter as the other stations (Figure 4). In contrast, [DO] at the under ice station was $<$90% at depths of 150–200 m (Figure 4), indicating significant respiration of organic matter at depth. These subsurface waters have temperature-salinity characteristics similar to the central Arctic and so this [DO] undersaturation may represent long-term respiration (i.e., respiration of organic matter not generated during the preceding bloom season). It is therefore challenging to compare the upper mesopelagic remineralization between ice influenced and non-ice influenced stations.

4.3.2. Heterotrophic Respiration

With enhanced organic matter availability, it can be expected that bacteria, as the main drivers of remineralization [*Giering et al.*, 2014], will increase in abundance and/or exhibit elevated metabolism. Within our study, examination of vertical profiles of bacterial activity (uptake of the amino-acid Leucine in this case; Figure 5a), bacterial abundance (Figure 5b), or heterotrophic flagellate abundance (Figure 5c) shows no clear enhancement below the 100 m depth horizon at any of the stations. In fact, the bacteria and heterotrophic flagellate abundance at depths of 100–300 m are within the same order of magnitude across all stations sampled (Figures 5b and 5c).

To a lesser extent, zooplankton also respire sinking carbon [*Giering et al.*, 2014]. Zooplankton oxygen respiration rates (Figure 7) were estimated from allometric relationships and biomass measurements of zooplankton species collected from surface nets (down to 200 m; see section 2 and supporting information Table S1). In the *P. pouchetii* bloom, the zooplankton respiration rate was low (Figure 7) relative to other stations, indicating no intense remineralization by zooplankton took place at the ice-edge station. However, zooplankton respiration was high at diatom dominated stations 10 and 42 as well as at station 19 where *P. pouchetii* was also present but not dominating biomass. Station 19 had not yet reached peak bloom at the time of sampling as revealed by the satellite Chl-*a* time series (Figure 3e). This open ocean site had lower biomass, PP and *P. pouchetii* abundance (Figure 1, Tables 1, and 2) and is in a typical prebloom state (e.g., PP is increasing but export has yet to start, see Figure 1b and Table 2). When in colonial blooming form as

observed at station 11, *Phaeocystis* can be a significant producer of dimethyl-sulfide (DMS) [*DiTullio et al*., 2000; *van Leeuwen et al*., 2007] and is repugnant to many marine grazers [*Schoemann et al*., 2005], which significantly increases its success and community dominance. The integrated (top 60 m) concentration of DMS at station 11 was almost twice as larger than at station 19 (523 and 331 nmol DMS m^{-2}, respectively) (F. Hopkins and J. Stephens, Plymouth Marine Laboratory, personal communication, 2012). This is a possible explanation for why at station 11 the zooplankton respiration rate is smaller than at station 19.

Although our approach only provides relative information and not quantitative rates of carbon remineralization at each station, several lines of evidence suggest that no enhanced remineralization of sinking material in the upper 300 m of the water column occurred below the *P. pouchetii* bloom (Stn. 11). Hence, the upper mesopelagic remineralization at the ice-edge bloom (Stn. 11) may have been similar to the diatom dominated stations and therefore, potentially as high as in diatom blooms in the North Atlantic that are amongst the highest observed globally [*Buesseler and Boyd*, 2009]. This trend also shows consistency in time as both bacterial/zooplankton remineralization rates and [DO] displays the same pattern. This suggests that the uniform remineralization (no matter the surface phytoplankton composition) we observed in the upper mesopelagic zone in the study region is not an artifact of decoupled integration time scales.

Extensive blooms of *Phaeocystis* spp. occur in the Southern Ocean [*Arrigo et al*., 1999; *DiTullio et al*., 2000; *Salter et al*., 2007] (*P. antarctica*) and in northern polar waters (*P. pouchetii*), such as the Barents Sea [*Reigstad and Wassmann*, 2007; *Smith et al*., 1991; *Wassmann et al*., 1990]. In the Ross Sea, observations from 300 to 500 m depth have previously suggested that *P. antarctica* is exported rapidly to depth with little remineralization through the upper water column [*DiTullio et al*., 2000]. Conversely, *P. pouchetii* blooms in the Barents Sea are thought to undergo more rapid remineralization in the upper water column than diatom blooms [*Reigstad and Wassmann*, 2007; *Wassmann et al*., 1990]. However, some recent observations suggest that ice-edge eddies can, on occasion, result in the export of *P. pouchetii* to depths greater than 340 m [*Lalande et al*., 2011].

Our results show that a high proportion of PP associated with a retreating ice-edge *P. pouchetii* bloom was exported below 100 m (high *ThE*-ratio), and, using [DO], bacterial/heterotrophic flagellate abundance/activity and zooplankton respiration rates, we infer that rates of remineralization of this material over the upper 100–350 m were similar to those found under diatom blooms. We only sampled one station (Stn. 11) where *P. pouchetii* was blooming; our results are therefore limited, but do highlight the potential for enhanced export related to the occurrence of Arctic *P. pouchetii*. We suggest that more effort be made to estimate accurately the carbon respiration rate under polar blooms of diatoms, coccolithophores and *Phaeocystis* spp. as none of the approaches cited above [*Buesseler and Boyd*, 2009; *DiTullio et al*., 2000; *Reigstad and Wassmann*, 2007] provide direct estimates of upper mesopelagic C remineralization rates in polar oceans.

5. Conclusions and Implications

Large uncertainties remain about the fate of sinking organic matter in the Arctic. This prevents reliable predictions of the strength of the BCP in the future Arctic Ocean. In June 2012, we surveyed the efficiency with which the biomass produced in the surface ocean was exported out of the sunlit layer of the ocean (the *ThE*-ratio [*Buesseler*, 1998]) and link it to the dominant phytoplankton group present in the water column. Furthermore, we compared several qualitative indicators of sinking material remineralization in the upper mesopelagic (>100 m). Our main conclusions are that:

1. Several phytoplankton blooms were observed during our survey: a *P. pouchetii* bloom at the ice edge in the Fram Strait, a diatom bloom in the Greenland Sea, and a bloom, where coccolithophores were present in the Norwegian and Barents Seas (Table 1).
2. Primary production and POC export were very low under the Greenland ice pack. The highest rates of POC export were recorded in an ice-edge bloom of *P. pouchetii* (Fram Strait) and in the south of the Greenland Sea near Iceland (Figure 1).
3. The *ThE*-ratio [*Buesseler*, 1998] displayed large spatial variability. The common denominator in stations where high *ThE*-ratio were recorded was the time of sampling relative to the seasonal bloom dynamics (e.g., all sampled during the main Chl-*a* peak or no more than a month after the main bloom peak). The

highest *ThE*-ratio was recorded in the mono-specific *P. pouchetii* bloom and in the diatom dominated stations near Iceland (Figure 3 and Table 3).

4. Our results suggest that, under certain circumstances, *Phaeocystis* blooms may experience little upper mesopelagic remineralization, as seen in diatom blooms.

Ultimately, the potential for phytoplankton bloom formation is driven by each species' ecological competitiveness [*Schoemann et al*., 2005], including its resistance to grazing. It is currently unclear whether the future Arctic Ocean PP is ultimately limited by light or nutrients; however, model predictions suggest that future Arctic primary production will be nutrient limited [*Vancoppenolle et al*., 2013]. Hence, although the behavior of grazers and the microbial community in the future Arctic is hard to forecast, predictions of a future reduction in nutrient concentrations in the Arctic [*Codispoti et al*., 2013], increased iron limitation due to reduction of ice cover [*Measures*, 1999] and possibly reduced stratification [*Carmack and Wassmann*, 2006], all suggest that there is potential for important changes in bloom composition in the future Arctic Ocean. In an increasingly ice-free Arctic Ocean [*Boé et al*., 2009; *Stroeve et al*., 2012], with a greater proportion of ice edge for bloom formation [*Perrette et al*., 2011], such fundamental processes will determine how climate change affects the strength of the Arctic carbon sink. We suggest that more effort is required to quantify the export ratio in the Arctic Ocean, and more importantly to assess the fate of sinking POC in the Arctic mesopelagic zone.

Acknowledgments

Katsiaryna Pabortsava, Richard Sanders, Jeff Benson, Andy Milton, Sinhue Torres-Valdes, Polly Hill (NOC), Frances Hopkins, John Stephens (PML), Mark Moore (University of Southampton), Eric Achterberg (GEOMAR Kiel/University of Southampton), and Robert Thomas (BODC) are acknowledged for help and advice. This research cruise could not have been undertaken without the efforts of a large number of people located in several organizations within the UK. We are grateful for the help and assistance of all those involved including: the Master Graham Chapman, officers and crew of the James Clark Ross; the scientists and technical support staff of cruise JR271; the staff of the British Antarctic Survey, Cambridge, National Marine Facilities, Southampton, and the Scottish Association for Marine Science, Oban. Raymond Leakey is warmly acknowledged for leading cruise JR 271 and scientific advice. We are also grateful to the UK Natural Environment Research Council (NERC), the UK Department of Environment, Food, and Rural Affairs (Defra), and the UK Department of Energy and Climate Change (DECC) for funding the research cruise via the UK Ocean Acidification research programme (NERC grant NE/H017097/1), and to the Danish, Icelandic, and Norwegian diplomatic authorities for granting permission to travel and work in Greenland, Iceland, and Svalbard coastal and offshore waters. We would like to thank two anonymous reviewers for providing constructive comments. This research was also funded by the NERC SeasFX project (grant NE/J004383/1). Data are held at the British Oceanographic Data Centre (http://bodc.ac.uk/).

References

Arrigo, K. R., G. van Dijken, and S. Pabi (2008), Impact of shrinking Arctic ice cover on marine primary production, *Geophys. Res. Lett.*, *35*, L19603, doi:10.1029/2008GL035028.

Arrigo, K. R., D. H. Robinson, D. L. Worthen, R. B. Dunbar, G. R. DiTullio, M. VanWoert, and M. P. Lizotte (1999), Phytoplankton community structure and the drawdown of nutrients and CO_2 in the Southern Ocean, *Science*, *283*(5400), 365–367.

Balch, W. M., D. T. Drapeau, and J. J. Fritz (2000), Monsoonal forcing of calcification in the Arabian Sea, *Deep Sea Res., Part II*, *47*, 1301–1337.

Baumann, M. S., S. B. Moran, M. W. Lomas, R. P. Kelly, and D. W. Bell (2013), Seasonal decloupling of particulate organic carbon export ans net primary production in relation to sea-ice at the shelf break of the eastern Bering Sea: Implications for off-shelf carbon export, *J. Geophys. Res. Oceans*, *118*, 5504–5522, doi:10.1002/jgrc.20366.

Benitez-Nelson, C., K. O. Buesseler, D. M. Karl, and J. Andrews (2001), A time-series study of particulate matter export in the North Pacific Subtropical Gyre based on Th-234:U-238 disequilibrium, *Deep Sea Res., Part I*, *48*(12), 2595–2611.

Boé, J., A. Hall, and X. Qu (2009), September sea-ice cover in the Arctic Ocean projected to vanish by 2100, *Nat. Geosci.*, *2*, 341–343, doi:10.1038/NGEO467.

Bopp, L., O. Aumont, P. Cadule, S. Alvain, and M. Gehlen (2005), Response of diatoms distribution to global warning and potential implications: A global model study, *Geophys. Res. Lett.*, *32*, L19606, doi:10.1029/2005GL023653.

Boyd, P., and P. Newton (1995), Evidence of the potential influence of planktonic community structure on the interannual variability of particulate organic-carbon dlux, *Deep Sea Res., Part I*, *42*(5), 619–639.

Boyd, P. W., and P. P. Newton (1999), Does planktonic community structure determine downward particulate organic carbon flux in different oceanic provinces?, *Deep Sea Res., Part I*, *46*(1), 63–91.

Boyd, P. W., and T. W. Trull (2007), Understanding the export of biogenic particles in oceanic waters: Is there consensus?, *Prog. Oceanogr.*, *72*(4), 276–312, doi:10.1016/j.pocean.2006.10.007.

Brix, H., N. Gruber, D. M. Karl, and N. R. Bates (2006), On the relationships between primary, net community, and export production in subtropical gyres, *Deep Sea Res., Part II*, *53*(5–7), 698–717.

Buesseler, K. O. (1998), The decoupling of production and particulate export in the surface ocean, *Global Biogeochem. Cycles*, *12*(2), 297–310.

Buesseler, K. O., and P. W. Boyd (2009), Shedding light on processes that control particle export and flux attenuation in the twilight zone of the open ocean, *Limnol. Oceanogr. Methods*, *54*(4), 1210–1232.

Buesseler, K. O., M. P. Bacon, J. K. Cochran, and H. D. Livingston (1992), Carbon and nitrogen export during the JGOFS North Atlantic bloom experiment estimated from ^{234}Th:^{238}U disequilibria, *Deep Sea Res., Part A*, *39*(7–8), 1115–1137.

Buesseler, K. O., J. A. Andrews, M. C. Hartman, R. Belastock, and F. Chai (1995), Regional estimates of the export flux of particulate organic carbon derived from thorium-234 during the JGOFS EqPac program, *Deep Sea Res., Part II*, *42*(2–3), 777–804.

Cai, P., M. Rutgers van der Loeff, I. Stimac, E. M. Nothig, K. Lepore, and S. B. Moran (2010), Low export flux of particulate organic carbon in the central Arctic Ocean as revealed by ^{234}Th:^{238}U disequilibrium, *J. Geophys. Res.*, *115*, C10037, doi:10.1029/2009JC005595.

Carmack, E., and P. Wassmann (2006), Food webs and physical-biological coupling on pan-Arctic shelves: Unifying concepts and comprehensive perspectives, *Prog. Oceanogr.*, *71*, 446–477, doi:10.1016/j.pocean.2006.10.004.

Cavalieri, D. J., C. L. Parkinson, P. Gloersen, and H. Zwally (1996, updated yearly), *Sea Ice Concentrations From Nimbus-7 SMMR and DMSP SSM/I-SSMIS Passive Microwave Data*, NASA DAAC at the Natl. Snow and Ice Data Cent., Boulder, Colo.

Cavan, E., F. A. C. Le Moigne, A. J. poulton, C. J. Daniels, G. Fragoso, and R. J. Sanders (2015), Zooplankton fecal pellets control the attenuation of particulate organic carbon flux in the Scotia Sea, Southern Ocean, *Geophys. Res. Lett.*, *41*, doi:10.1002/2014GL062744.

Chen, J. H., R. L. Edwards, and G. J. Wasserburg (1986), ^{238}U, ^{234}U and ^{232}Th in seawater, *Earth Planet. Sci. Lett.*, *80*(3–4), 241–251.

Chen, M., Y. P. Huang, P. G. Cai, and L. D. Guo (2003), Particulate organic carbon export fluxes in the Canada Basin and Bering Sea as derived from Th-234/U-238 disequilibria, *Arctic*, *56*(1), 32–44.

Codispoti, L. A., V. Kelly, A. Thessen, P. Matrai, S. Suttles, V. Hill, M. Steele, and B. Light (2013), Synthesis of primary production in the Arctic Ocean: III. Nitrate and phosphate based estimates of net community production, *Prog. Oceanogr.*, *10*(1), 126–150.

Coello-Camba, A., S. Agusti, J. Holding, J. M. Arrieta, and C. M. Duarte (2014), Interactive effect of temperature and CO_2 increase in arctic phytoplankton, *Front. Mar. Sci.*, *1*(49), doi:10.3389/fmars.2014.00049.

Coppola, L., M. Roy-Barman, P. Wassmann, S. Mulsow, and C. Jeandel (2002), Calibration of sediment traps and particulate organic carbon using ^{234}Th in the Barents Sea, *Mar. Chem.*, *80*(1), 11–26.
de Boyer Montegut, C., G. Madec, A. C. Fischer, A. Lazar, and D. Iudicone (2004), Mixed layer depth over the global ocean: An examination of profile data and a profile-based climatology, *J. Geophys. Res.*, *109*, C120003, doi:10.1029/2004JC002378.
Dickson, A. G. (1994), Determination of dissolved oxygen in sea water by Winkler titration, in *WHP 91-1: WOCE Operations Manual*, WOCE Hydrogr. Prog. Off., WOCE Operations Manual.
DiTullio, G. R., J. M. Grebmeier, K. R. Arrigo, M. P. Lizotte, D. H. Robinson, A. Leventer, J. B. Barry, M. L. VanWoert, and R. B. Dunbar (2000), Rapid and early export of *Phaeocystis antarctica* blooms in the Ross Sea, Antarctica, *Nature*, *404*(6778), 595–598.
François, R., S. Honjo, R. Krishfield, and S. Manganini (2002), Factors controlling the flux of organic carbon to the bathypelagic zone of the ocean, *Global Biogeochem. Cycles*, *16*(4), 1087, doi:10.1029/2001GB001722.
Giering, S. L. C., et al. (2014), Reconciliation of the carbon budget in the ocean's twilight zone, *Nature*, *507*(7493), 480–483.
Gradinger, R. R., and M. E. M. Baumann (1991), Distribution of phytoplankton communities in relation to the large-scale hydrographical regime in the Fram Strait, *Mar. Biol.*, *111*, 311–321.
Henson, S., R. Sanders, E. Madsen, P. Morris, F. A. C. Le Moigne, and G. Quartly (2011), A reduced estimate of the strength of the ocean's bioloical carbon pump, *Geophys. Res. Lett.*, *38*, L046006, doi:10.1029/2011GL046735.
Henson, S. A., R. J. Sanders, and E. Madsen (2012), Global patterns in efficiency of particulate organic carbon export and transfer to the deep ocean, *Global Biogeochem. Cycles*, *26*, GB1028, doi:10.1029/2011GB004099.
Henson, S. A., A. Yool, and R. J. Sanders (2015), Variability in efficiency of particulate organic carbon export: A model study, *Global Biogeochem. Cycles*, *29*, 33–45, doi:10.1002/2014GB004965.
Hill, V. J., P. A. Matrai, E. Olson, S. Suttles, M. Steele, L. A. Codispoti, and R. C. Zimmerman (2013), Synthesis of integrated primary production in the Arctic Ocean: II. In situ and remotely sensed estimates, *Prog. Oceanogr.*, *110*, 107–125.
Hopkins, T. S. (1991), The GIN Sea A synthesis of its physical oceanography and literature review 1972–1985, *Earth Sci. Rev.*, *30*, 175–318.
Ikeda, T., Y. Kanno, K. Ozaki, and A. Shimada (2001), Metabolic rates of epipelagic marine copepods as a function of body mass and temperature, *Mar. Biol.*, *139*, 587–596, doi:10.1007/S002270100608.
Kawakami, H., M. C. Honda, M. Wakita, and S. Watanabe (2007), Time-series observation of POC fluxes estimated from ^{234}Th in the northwestern North Pacific, *Deep Sea Res., Part I*, *54*, 1070–1090.
Koeve, W. (2001), Wintertime nutrients in the North Atlantic—New approaches and implications for new production estimates, *Mar. Chem.*, *74*(4), 245–260.
Lalande, C., E. Bauerfeind, and E. M. Nothig (2011), Downward particulate organic carbon export at high temporal resolution in the eastern Fram Strait: Influence of Atlantic water on flux composition, *Mar. Ecol. Prog. Ser.*, *440*, 127–136, doi:10.3354/meps09385.
Lalande, C., K. Lepore, L. W. Cooper, J. M. Grebmeier, and S. B. Moran (2007), Export fluxes of particulate organic carbon in the Chukchi Sea: A comparative study using ^{234}Th/^{238}U disequilibria and drifting sediment traps, *Mar. Chem.*, *103*(1), 185–196.
Lalande, C., S. B. Moran, P. Wassmann, J. M. Grebmeier, and L. W. Cooper (2008), ^{234}Th-derived particulate organic carbon fluxes in the northern Barents Sea with comparison to drifting sediment trap fluxes, *J. Mar. Syst.*, *73*(1–2), 103–113.
Lam, P. J., S. C. Doney, and J. K. B. Bishop (2011), The dynamic ocean biological pump: Insights from a global compilation of particulate organic carbon, $CaCO_3$ and opal concentrations profiles from the mesopelagic, *Global Biogeochem. Cycles*, *25*, GB3009, doi:10.1029/2010GB003868.
Le Moigne, F. A. C., S. A. Henson, R. J. Sanders, and E. Madsen (2013a), Global database of surface ocean particulate organic carbon export fluxes diagnosed from the ^{234}Th technique, *Earth Syst. Sci. Data*, *5*(2), 295–304, doi:10.5194/essd-5-295-2013.
Le Moigne, F. A. C., K. Pabortsava, C. L. J. Marcinko, P. Martin, and R. J. Sanders (2014), Where is mineral ballast important for surface export of particulate organic carbon in the ocean?, *Geophys. Res. Lett.*, *41*, 8460–8468, doi:10.1002/2014GL061678.
Le Moigne, F. A. C., M. Villa-Alfageme, R. J. Sanders, C. M. Marsay, S. Henson, and R. Garcia-Tenorio (2013b), Export of organic carbon and biominerals derived from ^{234}Th and ^{210}Po at the Porcupine Abyssal Plain, *Deep Sea Res., Part I*, *72*, 88–101, doi:10.1016/j.dsr.2012.10.010.
Loeng, H. (1991), *Features of the physical oceanographic conditions of the Barents Sea. Pp. S18 in Sakshaug*, edited by E. Hopkins, C. C. E. and N. A. Britsland, Proceedings of the Pro Mare Symposium on Polar Marine Ecology, Trondheim, 12–16 May 1990, Polar Research 10/1.
Martin, P., R. Lampitt, M. J. Perry, R. Sanders, C. Lee, and E. D'asaro (2011), Export and mesopelagic particle flux during a North Atlantic spring diatom bloom, *Deep Sea Res., Part I*, *58*(4), 338–349.
Measures, C. I. (1999), The role of entrained sediments in sea ice in the distribution of aluminium and iron in the surface waters of the Arctic Ocean, *Mar. Chem.*, *68*(1–2), 59–70.
Moran, S. B., K. M. Ellis, and J. N. Smith (1997), Th-234/U-238 disequilibrium in the central Arctic Ocean: Implications for particulate organic carbon export, *Deep Sea Res., Part II*, *44*(8), 1593–1606.
Moran, S. B., and J. N. Smith (2000), Super(234)Th as a tracer of scavenging and particle export in the Beaufort Sea, *Cont. Shelf Res.*, *20*(2), 153–167.
Pabi, S., G. L. van dijken, and K. R. Arrigo (2008), Primary production in the Arctic Ocean, 1998–2006, *J. Geophys. Res.*, *113*, C08005, doi:10.1029/2007JC004578.
Perrette, M., A. Yool, G. D. Quartly, and E. E. Popova (2011), Near-ubiquity of ice-edge blooms in the Arctic, *Biogeosciences*, *8*, 515–524, doi:10.5194/bg-8-515-2011.
Pike, S. M., K. O. Buesseler, J. Andrews, and N. Savoye (2005), Quantification of Th-234 recovery in small volume sea water samples by inductively coupled plasma-mass spectrometry, *J. Radioanal. Nucl. Chem.*, *263*(2), 355–360, doi:10.1007/s10967-005-0062-9.
Popova, E. E., A. Yool, A. C. Coward, Y. K. Aksenov, S. G. Alderson, B. A. de Cuevas, and T. R. Anderson (2010), Control of primary production in the Arctic by nutrients and light: Insights from a high resolution ocean general circulation model, *Biogeosciences*, *7*(11), 3569–3591.
Popova, E. E., A. Yool, A. C. Coward, F. Dupont, C. Deal, S. Elliott, E. Hunke, M. Jin, M. Steele, and J. Zhang (2012), What controls primary production in the Arctic Ocean? Results from an intercomparison of five general circulation models with biogeochemistry, *J. Geophys. Res.*, *117*, C00D12, doi:10.1029/2011JC007112.
Poulton, A., A. Charalampopoulou, J. R. Young, G. A. Tarran, M. I. Lucas, and G. D. Quartly (2010), Coccolithophore dynamics in non-bloom conditions during late summer in the central Iceland Basin (July-August 2007), *Limnol. Oceanogr. Methods*, *4*(55), 1601–1613.
Poulton, A. J., C. M. Moore, S. Seeyave, M. I. Lucas, S. Fielding, and P. Ward (2007), Phytoplankton community composition arounf the Crozet Plateau, with emphasis on diatoms and Phaeocystis, *Deep Sea Res., Part II*, *54*, 2085–2105.
Poulton, A. J., M. C. Stinchcombe, E. P. Achterberg, D. C. E. Bakker, C. Dumousseaud, H. E. Lawson, G. A. Lee, S. Richier, D. J. Suggett, and J. R. Young (2014), Coccolithophores on the north-west European shelf: Calcification rates and environmental controls, *Biogeosci. Discuss*, *11*, 2685–2733.
Reigstad, M., and P. Wassmann (2007), Does *Phaeocystis* spp. contribute significantly to verticalexport of organic carbon?, *Biogeochemistry*, *83*, 217–234, doi:10.1007/s10533-007-9093-3.

Reigstad, M., C. Wexels Riser, P. Wassmann, and T. Ratkova (2008), Vertical export of particulate organic carbon: Attenuation, composition and loss rates in the northern Barents Sea, *Deep Sea Res., Part II*, *55*, 2308–2319.
Resplandy, L., A. P. Martin, F. A. C. Le Moigne, P. Martin, A. Aquilina, L. Mémery, M. Lévy, and R. Sanders (2012), Impact of dynimical spatial variability on estimates of organic material export to the deep ocean, *Deep Sea Res., Part I*, *68*, 24–45.
Riley, J., R. Sanders, C. Marsay, F. A. C. Le Moigne, E. Achterberg, and A. Poulton (2012), The relative contribution of fast and slow sinking particles to ocean carbon export, *Global Biogeochem. Cycles*, *26*, GB1026, doi:10.1029/2011GB004085.
Rudels, B., G. Bjork, J. Nilsson, P. Winsor, I. Lake, and C. Nohr (2005), The interaction between waters from the Arctic Ocean and the Nordic Seas north of Fram Strait and along the East Greenland Current: Results from the Arctic Ocean-02 Oden expedition, *J. Mar. Syst.*, *55*, 1–30.
Rutgers van der Loeff, M. M., R. Meyer, B. Rudels, and E. Rachor (2002), Resuspension and particle transport in the benthic nepheloid layer in and near Fram Strait in relation to faunal abundances and Th-234 depletion, *Deep Sea Res., Part I*, *49*(11), 1941–1958.
Salter, I., R. S. Lampitt, R. Sanders, A. Poulton, A. E. S. Kemp, B. Boorman, K. Saw, and R. Pearce (2007), Estimating carbon, silica and diatom export from a naturally fertilised phytoplankton bloom in the Southern Ocean using PELAGRA: A novel drifting sediment trap, *Deep Sea Res., Part I*, *54*(18–20), 2233–2259, doi:10.1016/j.dsr2.2007.06.008.
Sanders, R., P. J. Morris, A. J. Poulton, M. C. Stinchcombe, A. Charalampopoulou, M. I. Lucas, and S. J. Thomalla (2010), Does a ballast effect occur in the surface ocean?, *Geophys. Res. Lett.*, *37*, L08602, doi:10.1029/2010GL042574.
Schoemann, V., S. Becquevort, J. Stefels, W. Rousseau, and C. Lancelot (2005), Phaeocystis blooms in the global ocean and their controlling mechanisms: A review, *J. Sea Res.*, *53*(1–2), 43–66, doi:10.1016/j.seares.2004.01.008.
Siegel, D. A., K. O. Buesseler, S. C. Doney, S. F. Sailley, M. J. Behrenfeld, and P. W. Boyd (2014), Global assessment of ocean carbon export by combining satellite observations and food-web models, *Global Biogeochem. Cycles*, *28*, 181–196, doi:10.1002/2013GB004743.
Smith, H. E. K. (2014), The contribution of mineralising phytoplankton to the biological carbon pump in high latitudes, PhD thesis, Univ. of Southampton, Southampton, U. K.
Smith, W. O., L. A. Codispoti, D. M. Nelson, T. Manley, E. J. Buskey, H. J. Niebauer, and G. F. Cota (1991), Importance of *Phaeocystis* blooms in the high latitude ocean carbon cycle, *Nature*, *352*, 514–516.
Smyth, T. J., T. Tyrrell, and B. Tarrant (2004), Time series of coccolithophore activity in the Barents Sea, from twenty years of satellite imagery, *Geophys. Res. Lett.*, *31*, L11302, doi:10.1029/2004GL019735.
Stroeve, J. C., V. Kattsov, A. Barrett, M. Serreze, T. Pavlova, M. Holland, and W. N. Meier (2012), Trends in Arctic sea ice extent from CMIP5, CMIP3 and observations, *Geophys. Res. Lett.*, *39*, L16502, doi:10.1029/2012GL052676.
Uttermohl, H. (1958), Zur vervollkommung der quantitativen phytoplankton methodik, *Int. Ver. Theor. Angew. Limnol.*, *9*, 38.
van Leeuwen, M. A., J. Stefels, S. Belviso, C. Lancelot, P. G. Verity, and W. W. C. Gieskes (2007), Phaeocystis, major link in the biogeochemical cycling of climate-relevant elements, *Biogeochemistry*, *83*, 1–3.
Vancoppenolle, M., L. Bopp, G. Madec, J. P. Dunne, T. Ilyina, P. R. Halloran, and N. Steiner (2013), Future Arctic Ocean primary productivity from CMIP5 simulations: Uncertain outcome, but consistent mechanisms, *Global Biogeochem. Cycles*, *27*, 605–619, doi:10.1002/gbc.20055.
Ward, P., A. Atkinson, and G. Tarling (2012), Mesozzoplankton community structure and variability in the Scotia Sea: A seasonal comparison, *Deep Sea Res., Part II*, 59–60.
Wassmann, P. (1994), Significance of sedimentation for the termination of Phaeocystis blooms, *J. Mar. Syst.*, *5*, 81–100.
Wassmann, P., M. Vernet, B. G. Mitchell, and F. Rey (1990), Mass sedimentation of *Phaeocystis pouchetii* in the Barents Sea, *Mar. Ecol. Prog. Ser.*, *66*, 183–195.
Woodgate, R. (2013), Arctic Ocean circulation: Going around at the top of the world, *Nat. Educ. Knowledge*, *4*(8), 8.
Zubkov, M. V., and P. H. Burkill (2006), Syringe pumped high speed flow cytometry of oceanic phytoplankton, *Cytometry Part A*, *69*, 1010–1019.
Zubkov, M. V., and G. A. Tarran (2008), High bacterivory by the smallest phytoplankton in the North Atlantic Ocean, *Nature*, *455*(7210), 224–226, doi:10.1038/nature07236.
Zubkov, M. V., M. A. Sleigh, P. H. Burkill, and R. J. G. Leakey (2000), Bacterial growth and grazing loss in contrasting areas of North and South Atlantic, *J. Plankton Res.*, *22*, 685–711.